Adaptive numerical homogenization of nonlinear diffusion problems

M. Bastidas, C. Bringedal, I.S. Pop, F.A. Radu

UHasselt Computational Mathematics Preprint
Nr. UP-19-04

April 16, 2019

ADAPTIVE NUMERICAL HOMOGENIZATION OF NON-LINEAR DIFFUSION PROBLEMS*

MANUELA BASTIDAS†, CARINA BRINGEDAL‡, IULIU SORIN POP†, AND FLORIN ADRIAN RADU§

Abstract. We propose an efficient numerical strategy for simulating fluid flow through porous media with highly oscillatory characteristics. Specifically, we consider non-linear diffusion models. This scheme is based on the classical homogenization theory and uses a locally mass-conservative formulation. In addition, we discuss some properties of the standard non-linear solvers and use an error estimator to perform a local mesh refinement. The main idea is to compute the effective parameters in such a way that the computational complexity is reduced without affecting the accuracy. We perform some numerical examples to illustrate the behaviour of the adaptive scheme and of the non-linear solvers. Finally, we discuss the advantages of the implementation of the numerical homogenization in a periodic media and the applicability of the same scheme in non-periodic test cases such as SPE10th project.

Key words. Flow in porous media, homogenization, upscaling, adaptive computations, non-linear solvers, MFEM.

AMS subject classifications. 35K55, 76S05, 76M50, 76M10.

1. Introduction.

Non-linear parabolic problems are encountered as mathematical models for several real life applications. Examples in this sense are partially saturated flow in porous media, non-steady filtration, and reaction-diffusion systems. Realistic applications often involve heterogeneous media, which translate into highly oscillatory coefficients and non-linearities. Letting Ω^ε be a bounded, possibly perforated domain in $\mathbb{R}^d$ $(d = 2, 3)$ with Lipschitz boundary and $\mathrm{T} > 0$ a maximal time with $\Omega^\varepsilon_\mathrm{T} := \Omega^\varepsilon \times (0, \mathrm{T}]$, we consider the non-linear diffusion equation

$$\partial_t b^\varepsilon(\mathbf{x}, p^\varepsilon(\mathbf{x}, t)) - \operatorname{div}\left(\mathbf{K}^\varepsilon(\mathbf{x})\,\nabla p^\varepsilon(\mathbf{x}, t)\right) = f^\varepsilon(\mathbf{x}, t), \quad \text{in } \Omega^\varepsilon_\mathrm{T}, \tag{1.1}$$

with suitable initial and boundary conditions.

In this setting, ε is a positive small parameter and denotes the scale separation between the micro-scale (e.g the scale of pores in a porous medium) and the macro-scale (e.g the Darcy scale, the scale of simulation in case of heterogeneous media). With the superscript $0 < \varepsilon \ll 1$ we indicate that the quantities involve highly oscillatory features and the medium is considered highly heterogeneous. Equation (1.1) can for example represent the non-dimensional Richards' equation after applying the Kirchhoff transformation and without taking into account gravity effects (see [7]). In this case, the primary unknown $p^\varepsilon(\mathbf{x}, t)$ is the transformation of the fluid pressure. For simplicity $p^\varepsilon(\mathbf{x}, t)$ will be called *pressure* in what follows. The given data include the source f^ε, the absolute permeability matrix $\mathbf{K}^\varepsilon$ and the volumetric fluid saturation b^ε, which is a given function of p^ε.

The development of numerical methods capturing the interaction between scales relies on high computational costs. The use of classical schemes over fine-scale meshes

*Submitted to the editors DATE.

Funding: This research is part of the Project G0G1316N *DynScale* funded through the *Odysseus* programme of the Research Foundation Flanders FWO in Belgium.

†Faculty of Sciences, Hasselt University. Diepenbeek, Belgium. (manuela.bastidas@uhasselt.be, uhasselt.be/CMAT).

‡Stuttgart Center for Simulation Technology (SimTech), University of Stuttgart. Stuttgart, Germany

§Department of Mathematics, University of Bergen. Bergen, Norway

has often unreachable requirements. To capture the oscillations in the medium the required mesh size would be very small compare to ε. In this sense, the standard numerical methods will either fail or become inefficient.

In consequence, there is a significant set of techniques for handling simulations that involve two or more scales in space and time. During the last years, approaches like the multi-scale finite-volume (MSFV), the algebraic dynamic multilevel (ADM) and the heterogeneous multi-scale (HMM) methods are becoming more and more relevant. Concretely, the MSFV and ADM methods proposed in [21, 22, 25] aim to solve problems involving different scales by incorporating the fine-scale variation into the coarse-scale operators. The multi-scale finite volume method (FVM) proposed in [22] is extended in [21] by including a dynamic local grid refinement method to provide accurate and efficient simulations employing fine grids only where needed. We highlight that the MSFV and ADM use a section of the fine-scale feature to construct the macro-scale solution without estimations of the macro-scale parameters. On the other hand, the HMM (see [3, 40]) relies on coupled macro and micro-scale solvers using homogenization (see [26]). This method takes advantage of the scale separation and is based on the numerical approximation of the macro-scale data. In [1, 2, 3] ideas on how to manage different scales in an efficient computational way are developed, using the standard finite element method (FEM). Further, the numerical computations using finite difference and discontinuous Galerkin method also demonstrate the potential of this framework in [18, 40].

Recently, many other works have proposed improved multi-scale methods to simulate non-linear single-phase and multi-phase flow. Among the recent literature, we emphasize the approaches in [5, 6, 23, 37, 41]. An Enhanced Velocity Mixed element method is proposed in [41] to deal with non-matching, multi-block grids and couple micro and macro scale domains. In the same line of research [6, 23, 37] give a computational strategy for the multi-scale dynamics over non-matching grids using mesh refinement and enriched multi-scale basis functions. In [5], the homogenization theory is combined with domain decomposition to obtain locally effective parameters and solve macro-scale problems.

In this paper, we develop a locally mass-conservative scheme that computes the homogenized permeability field of (1.1) over coarse meshes. In contrast with the papers mentioned before, we avoid the general grids and only use a-posteriori estimators on the macro-scale solvers. We propose a combination of techniques supported in the theoretical framework of the homogenization (see [26]) for non-linear parabolic equations. This strategy relies on the solution of micro-scale cell problems to calculate averaged parameters that one uses in a macroscopic solver. The focus of this work is to construct an efficient numerical strategy to approximate the solution of a non-linear and homogenized macro-scale model. It is important to remark that, despite the assumptions of periodicity that are needed in the classical homogenization theory, the advantages of this upscaling technique can be exploited even in the case of a non-periodic medium.

We apply the backward Euler (BE) method for the time discretization and the mixed finite element method (MFEM) for the spatial discretization. In order to solve the fully discrete formulation of (1.1), non-linear solvers are required. We discuss the applicability of classical iterative solvers like Newton or Picard (see [8, 17]) and we detail the formulation of a robust fixed point method called L-scheme proposed in [31].

This linearization procedure has the advantage of being unconditionally convergent. More exact, the convergence of the L-scheme is neither affected by the initial guess nor by the mesh size. Nevertheless, the convergence rate of the L-scheme is only linear and therefore slower compared to the Newton scheme (see [33]). We mention [28] for an approach combining the L and the Newton schemes in an optimized way. There, the L-scheme is applied to provide a suitable initial point for the Newton scheme. We use this strategy to improve the convergence of the scheme up to the quadratic convergence. We also refer to [29] for a modified L-scheme featuring improved convergence (compared to the L-scheme) and scalability properties (compared to Newton and Picard).

For time dependent problems the idea of adaptive meshes is very useful to localize the computational error. On the other hand, reaching finer meshes becomes computationally expensive because it requires extra calculations of the macro-scale parameters. The finer the mesh for the upscaled model, the higher the computational effort as the effective parameters need to be computed in more points, thus more cell problems need to be solved. For this reason, we present an a-posteriori estimator that indicates when the numerical solution and the effective parameters should be recomputed. With this strategy we aim to control the convergence rate of the numerical scheme and to avoid unnecessary computations of the local problems.

The main idea in this work is to exploit the advantages of the homogenization theory, adaptive mesh refinement and linearization procedures to obtain an efficient multi-scale solver for non-linear parabolic problems. The paper is organized as follows. In Section 2 the details of the model, the geometry and the discrete formulation are given and the necessary assumptions are stated. Section 3 gives a brief summary of the standard procedure of the homogenization for a parabolic case in a periodic porous media. There we also state the mixed and fully discrete formulation of the upscaled problem. In Section 4 the adaptive technique based on a-posteriori error estimators is introduced and in Section 5 the L-scheme is described. Finally, in Sections 6 and 7 we discuss numerical tests in the quasi-periodic and non-periodic case and some conclusions.

2. Model formulation and discretization. We consider the following non-linear parabolic problem, which appears on models of single-phase flow through a porous media

$$
\begin{aligned}
\partial_t b^\varepsilon(\mathbf{x}, p^\varepsilon(\mathbf{x},t)) - \operatorname{div}\left(\mathbf{K}^\varepsilon(\mathbf{x})\, \nabla p^\varepsilon(\mathbf{x},t)\right) &= f^\varepsilon(\mathbf{x},t), && \text{in } \Omega^\varepsilon_{\mathrm{T}},\\
p^\varepsilon(\mathbf{x},t) &= 0, && \text{on } \partial\Omega^\varepsilon_{\mathrm{T}},\\
p^\varepsilon(\mathbf{x},0) &= p_I(\mathbf{x}), && \text{in } \Omega^\varepsilon.
\end{aligned} \tag{2.1}
$$

Here Ω^ε is a bounded domain in $\mathbb{R}^d$ $(d = 2,3)$ with boundary $\partial\Omega^\varepsilon$. We denote $\Omega^\varepsilon_{\mathrm{T}} := \Omega^\varepsilon \times (0, \mathrm{T}]$ and let $\mathbf{n}$ being the unit normal pointing outwards of Ω^ε. Using the superscript $\varepsilon > 0$ we emphasize on the fact that rapidly oscillating characteristics are involved. For example, the domain either involves characteristics changing within ε-sized regions, or it may include perforation (like a porous medium).

Throughout this paper we use common notations from the functional analysis. By $L^p(\Omega^\varepsilon)$ we mean the space of the $p-$integrable functions with the usual norm. We let $\langle\cdot,\cdot\rangle$ represent the inner product on $L^2(\Omega^\varepsilon)$. For defining a solution in a weak sense we use the space $H^1_0(\Omega^\varepsilon) = \left\{p \in H^1(\Omega^\varepsilon) \,|\, p = 0 \text{ on } \partial\Omega^\varepsilon\right\}$ with $H^{-1}_0(\Omega^\varepsilon)$ being its dual.

We make the following assumptions:

(A1) The function $b^\varepsilon(\mathbf{x},\cdot)$ is non-decreasing, and $b^\varepsilon(\cdot,0) = 0$.

(A2) The function $b^\varepsilon(\mathbf{x},\cdot)$ is Hölder continuous: Constants $\alpha \in (0,1]$ and $L_b > 0$

exist such that

$$|b^\varepsilon(\mathbf{x}, p_1) - b(\mathbf{x}, p_2)| \le L_b |p_1 - p_2|^\alpha,$$

for all $\mathbf{x} \in \Omega^\varepsilon$ and $p_1,\, p_2 \in \mathbb{R}$.

(A3) The permeability function $\mathbf{K}^\varepsilon : \Omega^\varepsilon \to \mathbb{R}^{d\times d}$ is symmetric and continuous for all $\mathbf{x} \in \Omega^\varepsilon$. Further, the constants $\beta, \lambda > 0$ exist such that

$$\beta \|\psi\|^2 \le \psi^\intercal\, \mathbf{K}^\varepsilon(\mathbf{x})\, \psi \le \lambda \|\psi\|^2 \quad \text{for all } \psi \in \mathbb{R}^d \text{ and } \mathbf{x} \in \Omega^\varepsilon.$$

(A4) The initial data satisfies $p_I \in L^\infty(\Omega^\varepsilon_{\mathrm{T}})$ and the source term is $f^\varepsilon \in L^\infty(\Omega^\varepsilon_{\mathrm{T}})$.

A weak solution for the problem (2.1) is defined as

DEFINITION 2.1. *A function p^ε is called a weak solution of (2.1) if $\partial_t b^\varepsilon(\cdot, p^\varepsilon) \in L^2(0,\mathrm{T}; H_0^{-1}(\Omega^\varepsilon))$, $p^\varepsilon \in L^2(0,\mathrm{T}; H_0^1(\Omega^\varepsilon))$ and for all $\xi \in L^2(0,\mathrm{T}; H_0^1(\Omega^\varepsilon))$ it holds*

$$\int_0^{\mathrm{T}} \langle \partial_t b^\varepsilon, \xi \rangle_{H_0^{-1}(\Omega^\varepsilon)\times H^1(\Omega^\varepsilon)}\, dt + \int_0^{\mathrm{T}} \langle \mathbf{K}^\varepsilon(\boldsymbol{x})\, \nabla p^\varepsilon, \nabla \xi \rangle\, dt = \int_0^{\mathrm{T}} \langle f^\varepsilon, \xi \rangle\, dt.$$

We refer to [4] for the existence and uniqueness of the weak solution of the above problem. As a consequence one can also prove that $b^\varepsilon(\mathbf{x}, \cdot) \in L^\infty(0,\mathrm{T}; L^1(\Omega^\varepsilon))$ (see [4]).

2.1. Mixed formulation. In order to construct a robust and locally conservative scheme we consider the mixed formulation of (2.1). By defining $\mathbf{u}^\varepsilon(\mathbf{x})$ as the Darcy velocity, the unknowns $(p^\varepsilon, \mathbf{u}^\varepsilon) \in L^2(0,\mathrm{T}; H_0^1(\Omega^\varepsilon)) \times L^2(0,\mathrm{T}; H(\mathrm{div}, \Omega^\varepsilon))$ satisfy

$$\begin{aligned} \partial_t b^\varepsilon(\mathbf{x}, p^\varepsilon(\mathbf{x},t)) + \mathrm{div}\,(\mathbf{u}^\varepsilon(\mathbf{x},t)) &= f^\varepsilon(\mathbf{x},t), && \text{in } \Omega^\varepsilon_{\mathrm{T}},\\ \mathbf{u}^\varepsilon(\mathbf{x},t) &= -\mathbf{K}^\varepsilon(\mathbf{x})\, \nabla p^\varepsilon(\mathbf{x},t), && \text{in } \Omega^\varepsilon_{\mathrm{T}},\\ p^\varepsilon(\mathbf{x},t) &= 0, && \text{on } \partial\Omega^\varepsilon_{\mathrm{T}},\\ p^\varepsilon(\mathbf{x},0) &= p_I, && \text{in } \Omega^\varepsilon, \end{aligned} \tag{2.2}$$

with $H(\mathrm{div}, \Omega^\varepsilon) = \left\{ \mathbf{v} \in [L^2(\Omega^\varepsilon)]^d \,|\, \mathrm{div}(\mathbf{v}) \in L^2(\Omega^\varepsilon) \right\}$. It can be proved that the mixed variational formulation (2.2) is equivalent to the conformal formulation (2.1). We refer to [32] for the proof in both continuous and semi-discrete cases.

2.2. The non-linear fully discrete problem. To define the discrete problem we let $\mathfrak{T}_{h^\varepsilon}$ be a triangular partition of the domain Ω^ε with elements $\mathcal{T}$ of diameter $h^\varepsilon_{\mathcal{T}}$ and $h^\varepsilon := \max\limits_{\mathcal{T}\in\mathfrak{T}^\varepsilon_{h^\varepsilon}} h^\varepsilon_{\mathcal{T}}$ such that $h^\varepsilon \ll \varepsilon$. Further, $0 = t_0 \le t_1 \le t_1 \le \cdots \le t_N = \mathrm{T}$, $N \in \mathbb{N}$ is a partition of the time interval $[0, \mathrm{T}]$ with constant step size $\Delta t = t_{i+1} - t_i$, $i \ge 0$. For the discretization of the flux $\mathbf{u}^\varepsilon$ we consider the lowest-order Raviart-Thomas space $V_{h^\varepsilon} := \mathcal{RT}_0(\mathfrak{T}_{h^\varepsilon})$ and for the pressure p^ϵ we use the discrete subspace of piecewise constant functions W_{h^ε} (see [10]):

$$\begin{aligned} W_{h^\varepsilon} &:= \left\{ q \in L^2(\mathfrak{T}_{h^\varepsilon}) \,|\, q \text{ is constant on each element } \mathcal{T} \in \mathfrak{T}_{h^\varepsilon} \right\},\\ V_{h^\varepsilon} &:= \left\{ \mathbf{v} \in H_0(\mathrm{div}, \mathfrak{T}_{h^\varepsilon}) \,|\, \mathbf{v}|_{\mathcal{T}} = \mathbf{a} + b\mathbf{x} \text{ for all } \mathcal{T} \in \mathfrak{T}_{h^\varepsilon},\, \mathbf{a} \in \mathbb{R}^d,\, b \in \mathbb{R} \right\}. \end{aligned}$$

The fully discrete mixed finite element formulation of the problem (2.1) is

Problem $(\mathbf{PM}^\varepsilon_{\mathbf{n}})$. For a given $((p^\varepsilon)^{n-1}_{h^\varepsilon}, (\mathbf{u}^\varepsilon)^{n-1}_{h^\varepsilon}) \in W_{h^\varepsilon} \times V_{h^\varepsilon}$ and $n \ge 1$. Find $(p^\varepsilon)^n_{h^\varepsilon} \in W_{h^\varepsilon}$ and $(\mathbf{u}^\varepsilon)^n_{h^\varepsilon} \in V_{h^\varepsilon}$ such that for any $q \in W_{h^\varepsilon}$ and $\mathbf{v} \in V_{h^\varepsilon}$ there holds

$$\begin{aligned} \left\langle b^\varepsilon(\cdot, (p^\varepsilon)^n_{h^\varepsilon}) - b^\varepsilon\left(\cdot, (p^\varepsilon)^{n-1}_{h^\varepsilon}\right), q \right\rangle + \Delta t\, \langle \mathrm{div}\,((\mathbf{u}^\varepsilon)^n_{h^\varepsilon}), q \rangle &= \Delta t\, \langle f^\varepsilon, q \rangle,\\ \left\langle [\mathbf{K}^\varepsilon]^{-1}\, (\mathbf{u}^\varepsilon)^n_{h^\varepsilon}, \mathbf{v} \right\rangle - \langle (p^\varepsilon)^n_{h^\varepsilon}, \mathrm{div}\,(\mathbf{v}) \rangle &= 0. \end{aligned} \tag{2.3}$$

Where $(p^\varepsilon)^0_{h^\varepsilon}$ is the L^2-projection of the initial condition p_I over the mesh $\mathfrak{T}_{h^\varepsilon}$. For simplicity we omit writing the $\mathbf{x}$ argument in $b^\varepsilon(\mathbf{x}, p^\varepsilon)$, which becomes now $b^\varepsilon(p^\varepsilon)$. Here we assume that a solution to the discrete problem (2.3) exists and is unique. For details about this we refer the reader to [32, 35].

Note that the discrete problem (2.3) is non-linear, therefore a non-linear solver is needed. This is detailed in Section 5.

3. Two-scale approach: Periodic case. Consider Ω^ε as a bounded domain in $\mathbb{R}^d$ $(d = 2, 3)$ with Lipschitz boundary. We call *micro-scale* the region Y where the parameters change rapidly. In other words, the parameters and non-linearities take different values inside of Y (see Figure 1). In the extreme case, the micro-scale Y can be viewed as a perforated region with a pore space and a solid grain (see e.g [26]). Here we give the ideas for a non-perforated domains but this can be adapted straightforwardly to perforated ones.

At the micro-scale Y and the macro-scale Ω^ε we assume characteristic lengths ℓ and L respectively. The factor $\varepsilon := \frac{\ell}{L}$ denotes the scale separation between the two scales. To identify the variations at the micro-scale we define a fast variable $\mathbf{y} := \frac{\mathbf{x}}{\varepsilon}$. For each macro-scale point $\mathbf{x} \in \Omega^\varepsilon$ we use one micro-scale cell Y to capture the fast changes in the parameters.

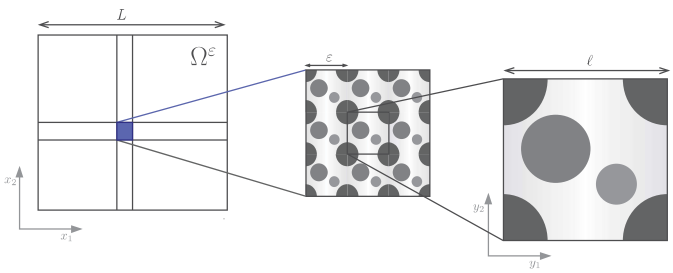

FIG. 1. *Two-scales scheme. Zoom in to the pore structure in $\mathbb{R}^2$ where typical length sizes and the multi-scale variables are indicated. (See [11]).*

In the non-dimensional setting, we assume that Ω^ε can be written as the finite union of the local cells $Y = [0, 1]^d$. To be specific, we let $\vec{i} \in \mathbb{Z}^d$ and $\Omega^\varepsilon = \cup \left\{ \varepsilon(\vec{i} + Y) \,|\, \vec{i} \in \mathcal{I}_\varepsilon \right\}$ for some set of vector indices $\mathcal{I}_\varepsilon$ and the outer boundary of Ω^ε is $\partial\Omega^\varepsilon$.

In order to formulate a homogenized problem, we make the following assumptions:

(B1) There exists a function $b : \Omega^\varepsilon \times \mathbb{R}^d \times \mathbb{R} \to \mathbb{R}$ such that $b^\varepsilon(\mathbf{x}, p^\varepsilon) := b(\mathbf{x}, \frac{\mathbf{x}}{\varepsilon}, p^\varepsilon)$ and $b(\mathbf{x}, \cdot, p^\varepsilon)$ is Y-periodic.

(B2) There exists a function $\mathbf{K} : \Omega^\varepsilon \times \mathbb{R}^d \to \mathbb{R}^{d\times d}$ such that $\mathbf{K}^\varepsilon(\mathbf{x}) := \mathbf{K}(\mathbf{x}, \frac{\mathbf{x}}{\varepsilon})$ where $\mathbf{K}(\mathbf{x}, \mathbf{y})$ is symmetric and continuous for all $(\mathbf{x}, \mathbf{y}) \in \Omega^\varepsilon \times Y$ and $\mathbf{K}(\mathbf{x}, \cdot)$ is Y-periodic. Further, the constants $\beta, \lambda > 0$ exist such that

$$\beta\|\psi\|^2 \le \psi^\mathsf{T}\, \mathbf{K}(\mathbf{x}, \mathbf{y})\, \psi \le \lambda\|\psi\|^2, \quad \text{for all } \psi \in \mathbb{R}^d, \mathbf{x} \in \Omega^\varepsilon \text{ and } \mathbf{y} \in Y.$$

Remark 3.1. Assumptions (B1) and (B2) are made in order to use the periodic homogenization theory for developing the multi-scale approach (see [20]). On the other hand, the assumptions (A1) to (A4) are required to formulate Theorem 3.2 (see [4, 12, 30]).

3.1. The homogenization approach. A direct numerical approximation of the problem (2.3) requires the usage of an extremely fine mesh to capture all the changes in the characteristics of the medium. In the following we consider an alternative approach and compute an effective model involving only the essential variations of the permeability matrix. Alternative approaches have also being considered, we refer to [36] for one involving the harmonic average of the parameters. Such techniques are rather suited for particular cases, e.g stratified media. However, our target is wider and the technique used here is mathematically consistent. We refer to [20, 26, 39] for a detailed presentation of the homogenization method.

Here, we restrict the presentation to the minimum needed for explaining the approach. We assume that all quantities satisfy the *homogenization ansatz* theory. For example p^ε can be formally expanded as power series in ε as

$$p^\varepsilon(\mathbf{x},t) = p_0(\mathbf{x},\mathbf{y},t) + \varepsilon p_1(\mathbf{x},\mathbf{y},t) + \varepsilon^2 p_2(\mathbf{x},\mathbf{y},t) + ... \tag{3.1}$$

where $\mathbf{y} = \frac{\mathbf{x}}{\varepsilon}$ stands for the fast variable, $\mathbf{x}$ is the slow variable and each function $p_i : \Omega^\varepsilon \times Y \times (0,T] \to \mathbb{R}$ is Y-periodic w.r.t $\mathbf{y}$. Additionally, the two-scale gradient and divergence operators become

$$\nabla = \nabla_x + \frac{1}{\varepsilon}\nabla_y \quad \text{and} \quad \text{div} = \text{div}_x + \frac{1}{\varepsilon}\text{div}_y.$$

Using (3.1), the two-scale operators and since $b(\mathbf{x},\mathbf{y},p^\varepsilon) = b^\varepsilon(\mathbf{x},p^\varepsilon)$ one applies the Taylor expansion of $b(\cdot,\cdot,p)$ about p_0 to obtain

$$\partial_t b - \left(\text{div}_x + \frac{1}{\varepsilon}\text{div}_y\right)\left(\mathbf{K}\left(\nabla_x + \frac{1}{\varepsilon}\nabla_y\right)\left(p_0 + \varepsilon p_1 + \varepsilon^2 p_2\right)\right) + \mathcal{O}(\varepsilon) \; = \; f. \tag{3.2}$$

Equating similar terms in ε one gets that $p_0 = p_0(\mathbf{x},t)$ does not depend on $\mathbf{y}$ and is in fact the *macro-scale approximation* of the pressure $p^\varepsilon(\mathbf{x},t)$.

To determine p_1 as a function of p_0, for the terms of order $\mathcal{O}(\varepsilon^{-1})$ we can write $p_1(\mathbf{x},\mathbf{y},t) = \hat{p_1}(\mathbf{x},t) + \sum_{j=1}^d \frac{\partial p_0(\mathbf{x},t)}{\partial x_j}\,\omega^j(\mathbf{x},\mathbf{y})$ where the function $\hat{p_1}$ is an arbitrary function of $\mathbf{x}$ and ω^j are the Y-periodic solutions of the following *micro-cell* problems

$$-\nabla_y \cdot \left(\mathbf{K}(\mathbf{x},\mathbf{y})\,\left(\nabla_y\omega^j + \mathbf{e}_j\right)\right) = 0, \text{ for all } \mathbf{y} \in Y. \tag{3.3}$$

Here $\{\mathbf{e}_j\}_{j=1}^d$ is the canonical basis of dimension d. To guarantee the uniqueness of the solution we assume that ω^j has the average 0 over the micro cells, that is, $\int_Y \omega^j(\mathbf{x},\mathbf{y}) = 0$ for all $\mathbf{x} \in \Omega$.

To simplify the notation in the following we use p instead of p_0 for the *macro-scale approximation* of the pressure p^ε. Recalling the boundary conditions on the micro-scale, the terms of order zero in (3.2) and averaging over Y one obtains the following *homogenized problem*

$$\begin{aligned} \partial_t b^\star(\mathbf{x},p) - \text{div}\left(\mathbf{K}^\star(\mathbf{x})\,\nabla p\right) &= f^\star(\mathbf{x},t), && \text{in } \Omega_{\mathrm{T}} := \Omega \times (0,\mathrm{T}], \\ p &= 0, && \text{on } \partial\Omega, \\ p(\mathbf{x},0) &= p_I, && \text{in } \Omega. \end{aligned} \tag{3.4}$$

The effective permeability $\mathbf{K}^\star : \Omega \to \mathbb{R}^{d\times d}$ has the elements

$$\mathbf{K}^\star_{i,j}(\mathbf{x}) = \int_Y \left(\mathbf{K}(\mathbf{x},\mathbf{y})\left(\mathbf{e}_j + \nabla_y\omega^j(\mathbf{x},\mathbf{y})\right)\right)\cdot \mathbf{e}_i\,d\mathbf{y}, \quad (i,j = 1,\dots d).$$

The upscaled saturation and source are

$$b^\star(\mathbf{x},p) := \int_Y b(\mathbf{x},\mathbf{y},p)\,d\mathbf{y} \quad \text{and} \quad f^\star(\mathbf{x},t) := \int_Y f(\mathbf{x},\mathbf{y},t)\,d\mathbf{y}.$$

The difference between the original problem (2.1) and the approximated problem (3.4) is subtle. In the original problem, the main characteristics are present at all scales, in the complex domain and in a strongly coupled manner. The *homogenized model* instead involves only essential variations at the macro-scale. However, to determine the value of the permeability tensor at a macro point $\mathbf{x} \in \Omega$, one has to solve d micro-cell problems (3.3) associated with that macro point. Note that these problems reflect the rapidly oscillating characteristics and are decoupled from the macro-scale variations. From a computational point of view, the importance of this decoupling becomes obvious. Instead of solving the full problem, one solves a collection of simpler problems. In general, analytic solutions are not available to compute the homogenized parameters. Then $\mathbf{K}^\star$, $b^\star$ and $f^\star$ must usually be computed numerically and can therefore only be obtained at discrete points of the domain Ω. This strategy was also used in [1, 3, 5].

Concerning the existence and uniqueness of the weak solution of the homogenized problem (3.4) we use the assumptions (A1) to (A4) and assumptions (B1) and (B2) and refer to [4]. More precisely if there exists a constant $\theta > 0$ such that, for every δ and R with $0 < \delta < R$ there exists $C(\delta, R) > 0$ such that

$$|b(\mathbf{x}, \mathbf{y}, \rho_1) - b(\mathbf{x}, \mathbf{y}, \rho_2)| \geq C(\delta, R)|\rho_1 - \rho_2|^\theta,$$

for all $\mathbf{x} \in \Omega^\varepsilon$, $\mathbf{y} \in Y$ and ρ_1, $\rho_2 \in [-R, R]$ with $\delta < |\rho_1|$, then the strong convergence of p^ε to p is showed in the following theorem (see [12, 27, 30] for the proof).

THEOREM 3.2. *Let p^ε be a family of solutions of the problem (2.1). If p^ε is such that $\sup_\varepsilon \|p^\varepsilon\|_{L^\infty(\Omega^\varepsilon_T)} \leq C$ with $C > 0$ and under the assumptions (A1)-(A4) and (B1)-(B2), there exists a subsequence of p^ε, still denoted by p^ε, such that for all q with $0 < q < \infty$, we have, $p^\varepsilon \to p$ strongly in $L^q(\Omega_\mathrm{T})$, where p solves (3.4).*

Following the ideas mentioned in Section 2, defining $\mathbf{u}(\mathbf{x})$ as the upscaled Darcy velocity, the upscaled unknowns $(p, \mathbf{u}) \in L^2(\Omega) \times H(\mathrm{div}, \Omega)$ satisfy

$$\begin{aligned} \partial_t b^\star(\mathbf{x}, p(\mathbf{x}, t)) + \mathrm{div}\,(\mathbf{u}(\mathbf{x}, t)) &= f^\star(\mathbf{x}, t), && \text{in } \Omega_\mathrm{T}, \\ \mathbf{u}(\mathbf{x}, t) &= -\mathbf{K}^\star(\mathbf{x})\,\nabla p(\mathbf{x}, t), && \text{in } \Omega_\mathrm{T}, \\ p(\mathbf{x}, t) &= 0, && \text{on } \partial\Omega, \\ p(\mathbf{x}, 0) &= p_I, && \text{in } \Omega. \end{aligned} \tag{3.5}$$

Remark 3.3. If the original permeability $\mathbf{K}^\varepsilon$ satisfies (B2) then the effective tensor $\mathbf{K}^\star$ is also symmetric and positive definite. Nevertheless, in the case of an initial isotropic medium the effective permeability can contains anisotropies, (e.g the tensor could be non-diagonal). However, in this case the non-diagonal components of $\mathbf{K}^\star$ are neglectable and the diagonal elements are similar.

The non-linear discrete problem associated with the homogenized formulation (3.5) is defined in the following.

3.2. The non-linear fully discrete homogenized problem. Let $\mathfrak{T}_H$ be a coarse-triangular partition of the domain Ω with coarse elements $\mathcal{T}$ of diameter $H_\mathcal{T}$ and $H := \max_{\mathcal{T} \in \mathfrak{T}_H} H_\mathcal{T}$. For the discretization of the flux $\mathbf{u}$ we consider the lowest-order Raviart-Thomas space $V_H := \mathcal{R}T_0(\mathfrak{T}_H)$ and for the pressure p we use the discrete subspace of piecewise constant functions W_H (see [10]).

Problem $(\mathbf{PH_n})$. For a given $(p_H^{n-1}, \mathbf{u}_H^{n-1}) \in W_H \times V_H$ and $n \geq 1$, find $p_H^n \in W_H$ and $\mathbf{u}_H^n \in V_H$ such that for any $q_H \in W_H$ and $\mathbf{v}_H \in V_H$ there holds

$$\begin{aligned} \left\langle b^\star\left(\cdot, p_H^n\right) - b^\star\left(\cdot, p_H^{n-1}\right), q_H\right\rangle + \Delta t \left\langle \operatorname{div}\left(\mathbf{u}_H^n\right), q_H\right\rangle &= \Delta t \left\langle f^\star, q_H\right\rangle, \\ \left\langle \left[\mathbf{K}^\star\right]^{-1} \mathbf{u}_H^n, \mathbf{v}_H\right\rangle - \left\langle p_H^n, \operatorname{div}\left(\mathbf{v}_H\right)\right\rangle &= 0. \end{aligned} \tag{3.6}$$

Again p_H^0 is the L^2-projection of the initial p_I over the coarse mesh $\mathfrak{T}_H$. For simplicity we omit writing the $\mathbf{x}$ argument in $b^\star(\mathbf{x}, p)$, which becomes now $b^\star(p)$. If $b(\mathbf{x}, \mathbf{y}, p_H^n)$ has no micro-scale dependence $b^\star(p_H^n) = |P|\, b(\mathbf{x}, p_H^n)$ and the same argument applies for $f^\star$.

3.3. Micro-cell problem and micro-scale discretization. As mentioned before, the effective parameters must be computed at each integration point on the coarse triangulation $\mathfrak{T}_H$. The effective tensor $\mathbf{K}^\star$ depends on the solution of the micro cell problems (3.3). To solve (3.3) we use the same MFEM scheme as for (3.4).

To approximate the solution of (3.3) we use a triangular decomposition $\mathfrak{T}_h$ of the micro-scale domain $P \subseteq Y$ with micro-scale mesh size h. For each integration point $\mathbf{x} \in \mathcal{T}$ and $\mathcal{T} \in \mathfrak{T}_H$, the discrete micro-cell problem is

Problem $(\mathbf{Ph_j})$. Find $(\omega_h^j, \vec{\xi}_h^j) \in W_h \times V_h$ satisfying

$$\begin{aligned} \left\langle \operatorname{div}\left(\vec{\xi}_h^j\right), q_h\right\rangle &= \left\langle f, q_h\right\rangle, \\ \left\langle \left[\mathbf{K}(\mathbf{x}, \cdot)\right]^{-1} \vec{\xi}_h^j, \mathbf{v}_h\right\rangle - \left\langle \omega_h^j, \operatorname{div}\left(\mathbf{v}_h\right)\right\rangle &= 0, \\ \omega_h^j \text{ is } Y-\text{periodic}, & \end{aligned} \tag{3.7}$$

for all $q_h \in W_h$, $\mathbf{v}_h \in V_h$ and $j = 1, \ldots, d$.

After solving (3.7) we can compute the discrete effective permeability: $\mathbf{K}^\star_{i,j}(\mathbf{x}) = \left(\int_Y \left(\mathbf{K}(\mathbf{x}, \mathbf{y}) \left(\mathbf{e}_j + \vec{\xi}_h^j(\mathbf{y})\right)\right) \cdot \mathbf{e}_i \, d\mathbf{y}\right)$ and use it to solve the discrete problem (3.6). Note that these cell problems only need to be solved initially, or when the mesh changes.

4. Adaptive numerical homogenization. The standard homogenization theory applies for periodic media although its extension to random media is well understood (see e.g [2]). In practical cases, one does not have any structure in the oscillations of the data. Nevertheless the computation of macro-scale parameters remains a suitable idea. We propose to solve the micro-cell problems (3.7) and compute the macro-scale parameters over a coarse mesh defined by the user. This procedure consists in two steps:

- *The macro-scale partition*: Define a macro-scale division of the domain Ω with elements Q_k, $(k = 1, 2, \ldots, m)$, where m is the total number of coarse cells.
- *The micro-scale domains*: Solve the micro-cell problems (3.7) over each coarse element Q_k. Note that Q_k determines a micro-scale domain and there we define a micro-scale mesh size h. The upscaled permeability that belongs to each region Q_k highly depends on the choice of h.

Subsequently one can mesh the macro-scale domain and solve the homogenized problem (3.4). In Figure 2 we show the configuration of the macro and micro-scale partition and the procedure described previously. Note that neither the macro-scale partition nor the micro-scale mesh needs to be uniform.

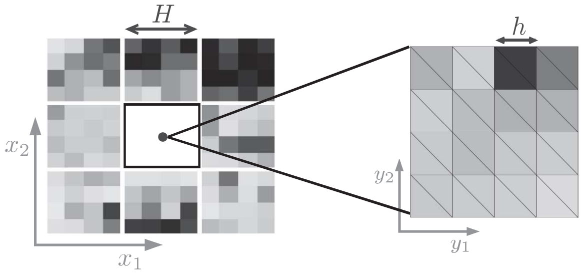

FIG. 2. *Sketch of the macro-scale partition and the correspondent micro-scale discretization in a domain $\Omega \subset \mathbb{R}^2$. Different colours represent different values of the permeability.*

4.1. A-posteriori error estimates. In the following we propose a four-step strategy to localize the error of the numerical solution of the homogenized problem. For this reason, it is necessary to compute a local error estimator $\eta_{\mathcal{T}}$ at each element $\mathcal{T} \in \mathfrak{T}_{H_n}$. Choosing an error estimator $\eta^n_{\mathcal{T}}$ highly depends on the features of each numerical method, the approximation, the post processing strategy, the implementation etc. Nevertheless, we refer to [14], where the equivalence between different a-posteriori error estimators is analysed.

In the *error control based on averaging technique* [13, 15] the idea is to estimate the error based on a smoother approximation to the discrete solution $\mathbf{u}^n_H$. We define a global error estimator η_Ω and an average operator $\mathfrak{A}_z$

$$\eta_\Omega := \min_{\mathbf{v}\in V_h} \|\mathbf{u}^n_H - \mathbf{v}\|_{L^2(\Omega)} \quad \text{and} \quad \mathfrak{A}\mathbf{u}^n_H(z) = \mathfrak{A}_z(\mathbf{u}^n_H) := \frac{1}{|w_z|}\int_{w_z} \mathbf{u}^n_H \, d\mathbf{x}$$

where $w_z := \text{int}\,(\cup\{\mathcal{K} \in \mathfrak{T}_{H_n} : \mathcal{K} \cap \mathcal{T} \neq \emptyset, z \in \mathcal{T}\})$ is the patch corresponding to the point $z \in \Omega$. It has been proven (see [13]) that the error $\|\mathbf{u}^n - \mathbf{u}^n_H\|_{L^2(\Omega)}$ is bounded by $\|\mathbf{u}^n_H - \mathbf{v}\|_{L^2(\Omega)}$ for any continuous and piecewise polynomial $\mathbf{v}$. Then an upper bound of η_Ω can be computed as

$$\|\mathbf{u}^n - \mathbf{u}^n_H\|_{L^2(\Omega)} \le C\eta_\Omega + \text{h.o.t} \le C\|\mathbf{u}^n_H - \mathfrak{A}\mathbf{u}^n_H\|_{L^2(\Omega)} + \text{h.o.t} \tag{4.1}$$

for some $C > 0$ independent of the mesh size. After choosing this estimator and in order to find the *optimal* macro-scale division to compute the effective parameters, as well as the solution of the homogenized problem (3.4) we will use a mesh adaptivity strategy.

4.2. Mesh adaptivity. We continue with a mesh adaptivity process using the a-posteriori estimator (4.1). Our approach consists of the sequence: Solve - estimate the error - select the cells/triangles - refine the mesh. The mesh refining generates a sequence of triangular meshes (one mesh per time step).

- (S1) *Solve*: The starting point is an initial coarse mesh $\mathfrak{T}_{H_1}$ and the approximation of the pressure and velocity $(p^1_H, \mathbf{u}^1_H)$ that satisfy the discrete problem (3.6) in the first time step.
- (S2) *Estimate the error*: Let the solution $(p^n_H, \mathbf{u}^n_H)$ over $\mathfrak{T}_{H_n}$ be given. Locally, an upper bound error estimator can be computed using the element-wise contributions in (4.1), i.e $(\eta^n_{\mathcal{T}}) := \|\mathbf{u}^n_H - \mathfrak{A}\mathbf{u}^n_H\|_{L^2(\mathcal{T})}$.
- (S3) *Select the cells/triangles*: An *optimal* mesh corresponds to a mesh where the error is equidistributed. For this reason, the elements marked to be refined are $\mathcal{T} \in \mathfrak{T}_{H_n}$ such that (see [16])

$$\eta^n_{\mathcal{T}} \ge \Theta\left(\max_{\mathcal{K}\in\mathfrak{T}_{H_n}} \eta^n_{\mathcal{K}}\right) \quad \text{with } \Theta \in (0,1).$$

(S4) *Refine the mesh*: The last step of the refinement corresponds to including new points and re-mesh. Our strategy avoids the possibility of nonconforming meshes. We refine each selected cell in four new cells to compute four new the effective permeabilities. Inside of the new finer cells we re-mesh with the necessary triangles.

The outline of the steps (S1) to (S4) is presented in Figure 3 for the 2D case and in 3D the refinement can be done as described in [24]. In Figure 3 we highlight that at every time step it is necessary to make sure that in the new mesh each element corresponds only to one permeability value. That restriction forces us to refine also neighbouring elements and increases the resolution of the numerical solution.

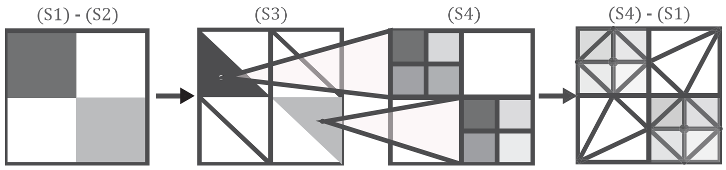

FIG. 3. *Outline of the a-posteriori refinement in $\mathbb{R}^2$. (Left to right) Initial effective permeability. Initial triangulation and selected triangles to refine. Refinement of the permeability field. Refinement of the triangular mesh.*

With this strategy we allow to have more than one level of refinement, although the homogenization theory only consider two levels. The threshold for the refinement Θ can be chosen depending on the problem. We remark that higher values of Θ remain into coarser meshes and less error control. In the numerical examples we show how the refinement increase the accuracy of the parameters and the upscaled solution.

5. Linearization.

A popular strategy to solve non-linear problems is Newton's method (see [8]). The reason to use Newton's method is the quadratic convergence, but we remark that quadratic convergence only arises under certain restrictions and it is only locally convergent. For the Newton method, the initial guess for the iterations must to be close enough to the expected solution for the scheme to be convergent. For all these reasons, we will also use a fixed point iteration scheme, called L-scheme. Although the L-scheme is only linearly convergent, it has unconditional convergence, meaning that it converges to the time-discrete solution regardless of the initial point and it does not involve any derivatives (see [34, 31, 38]).

For a $\mathfrak{L} \geq \max_{p\in\mathbb{R}} \{\partial_p b^\star(\cdot,p)\}$, assume p_H^{n-1} given. With $i \in \mathbb{N}$, $i \geq 1$ being the iteration index, the L-Scheme is introduced through: *Find $p_H^{n,(i)} \in W_H$ and $\boldsymbol{u}_H^{n,(i)} \in V_H$ such that for any $q_H \in W_H$ and $\boldsymbol{v}_H \in V_H$ there holds*

$$\begin{aligned} &\left\langle \mathfrak{L}\left(p_H^{n,(i)} - p_H^{n,(i-1)}\right) + b^\star\left(\cdot, p_H^{n,(i-1)}\right), q_H \right\rangle \\ &\qquad + \Delta t \left\langle \operatorname{div}\left(\mathbf{u}_H^{n,(i)}\right), q_H \right\rangle = \Delta t \left\langle f^\star, q_H \right\rangle + \left\langle b^\star(\cdot, p_H^{n-1}), q_H \right\rangle, \\ &\left\langle \mathbf{u}_H^{n,(i)}, \mathbf{v}_H \right\rangle - \left\langle \mathbf{K}^\star\, p_H^{n,(i)}, \operatorname{div}(\mathbf{v}_H) \right\rangle = 0. \end{aligned} \tag{5.1}$$

Where the natural choice for the initial iteration $p_H^{n,0}$ is p_H^{n-1}. In our non-linear solver the iterations take place until one reaches a prescribed threshold for the L^2-norm of the residual $\partial p_H^{n,i} := p_H^{n,(i)} - p_H^{n,(i-1)}$.

The use of an upper bound of $\partial_p b^\star(\cdot,p)$ affects the convergence rate. For the L-scheme the convergence rate is $\alpha = \frac{\mathfrak{L}-m}{\mathfrak{L}+C\Delta t}$ for some $C > 0$ and $m < \mathfrak{L}$ (see [31]).

This leads to an extremely slow convergences in some cases (e.g large $\mathfrak{L}$ or small Δt). For this reason in Section 6 we choose a smaller value $\mathfrak{L} = \frac{1}{2}\max_{p\in\mathbb{R}}\{\partial_p b^\star(\cdot, p)\}$ which still gives convergence (see [28]). For more results and analysis of the linearization techniques we refer to [31, 28] and therein references.

6. Numerical results. We present two numerical examples in $\mathbb{R}^2$ to illustrate the behaviour of the proposed adaptive homogenization procedure. We first verify our numerical homogenization approach using a manufactured periodic and quasi-periodic media and subsequently use a non-periodic test case. Note that all parameters specified in the following examples are non-dimensional and the pressures are also shifted to lie between 0 and 1.

6.1. Periodic and quasi-periodic cases. Consider the macro-scale domain $\Omega = [0, 1] \times [0, \frac{1}{2}]$ with initial condition $p_0 = 0$ and no-flux boundary conditions. The isotropic periodic permeability field is defined by

$$\mathbf{K}^\varepsilon(\mathbf{x}) = \left(10x_1^2 x_2 + \frac{1}{2 + 1.8\cos(2\pi\frac{x_1}{\varepsilon})\cos(2\pi\frac{x_2}{\varepsilon})}\right)\mathbb{I}_{2\times 2}$$

A source and a sink are placed in the upper-right and the lower-left corners, having fixed pressures of 1 and 0, respectively. The volumetric concentration is $b^\varepsilon(\mathbf{x}, p) = \mathcal{R}(p^\varepsilon)^3$. Here $\mathcal{R}$ is a non-dimensional constant that let us simulate a *fast diffusion* process. For the time discretization we take $T = 1$ with $\Delta t = 0.02$.

To solve the problem (5.1) with the necessary resolution to capture the oscillations over Ω the mesh size is restricted to be $h^\varepsilon \ll \varepsilon$. We use $h^\varepsilon = 5\times 10^{-3}$ to compute the fine-scale solutions $(p_{h^\varepsilon}, \mathbf{u}_{h^\varepsilon})$ when $\varepsilon = \frac{1}{8}, \frac{1}{16}$ and $\frac{1}{32}$. The reference solutions are computed using the same MFEM, backward Euler scheme and the L-scheme with $\mathfrak{L} = 1.5\frac{\mathcal{R}}{2} \geq \frac{\max\left(3\mathcal{R}(p^\varepsilon)^2\right)}{2}$.

Table 1 shows the history of convergence of the error for different values of ε and three coarse meshes $\mathfrak{T}_H$ without refinement and $H \gg h^\epsilon$. The relative L^2-error e_H in Table 1 is $e_H = \|\Pi_{h^\varepsilon}(p_H) - p_h\|_{L^2(\mathfrak{T}_{h^\varepsilon})} / \|p_h\|_{L^2(\mathfrak{T}_{h^\varepsilon})}$ where $\Pi_{h^\varepsilon}(p_H)$ is the projection of the coarse-scale solution in the fine mesh $\mathfrak{T}_{h^\varepsilon}$. With this result we show that the homogenized solution converges to the solution of the original problem when $H \to 0$ and also when $\varepsilon \to 0$.

Nevertheless, in the following we use a modified permeability field to ensure that any assumption of periodicity is necessary. We include in the same domain Ω a high permeability region Ω_1 and a low permeability region Ω_2 where the permeability is 10^{-2} and 10^{-7} respectively.

$$\Omega_1 := [0.21, 0.41] \times [0.11, 0.41] \text{ and } \Omega_2 := \left\{\mathbf{x} \in \Omega^\varepsilon \mid \|\mathbf{x} - [0.75, 0.26]\|_2 \leq 0.1^2\right\}.$$

In Figure 4 the normalized (quasi-periodic) permeability field is showed for two values of the scale parameter ε. In this case the boundary conditions, the volumetric concentration, the source term and the time discretization remain the same as before. Figure 5 shows four levels of the first component of the effective permeability tensor $(\mathbf{K}^\star_{1,1})$ starting with a coarse grid of 16×8 cells. Referring to the different levels of the effective permeabilities is important to remark that the coarse-scale permeabilities are computed in zones that not always match with the initial resolution or periodicity. Here one can notice the influence of neighbouring macro-cells in the numerical solution of the micro problems (3.7). This effect is evident at the boundary of the low permeability zone Ω_2. To point out this behaviour in the Figure 5 we highlight

ε	H	Relative error (e_H)
$1/8$	0.1768	0.1938
$1/8$	0.0884	0.1287
$1/8$	0.0442	0.0856
$1/16$	0.1768	0.1797
$1/16$	0.0884	0.1138
$1/16$	0.0442	0.0724
$1/32$	0.1768	0.1690
$1/32$	0.0884	0.1030
$1/32$	0.0442	0.0621

TABLE 1
History of convergence of the error for three values of ε and three coarse meshes.

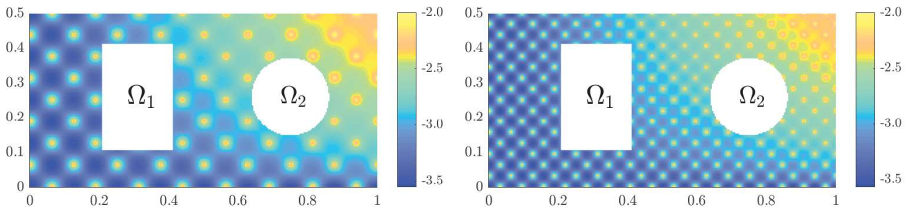

FIG. 4. *Fine scale permeability field (left) $\varepsilon = \frac{1}{8}$ and (right) $\varepsilon = \frac{1}{16}$ (Log_{10} scale).*

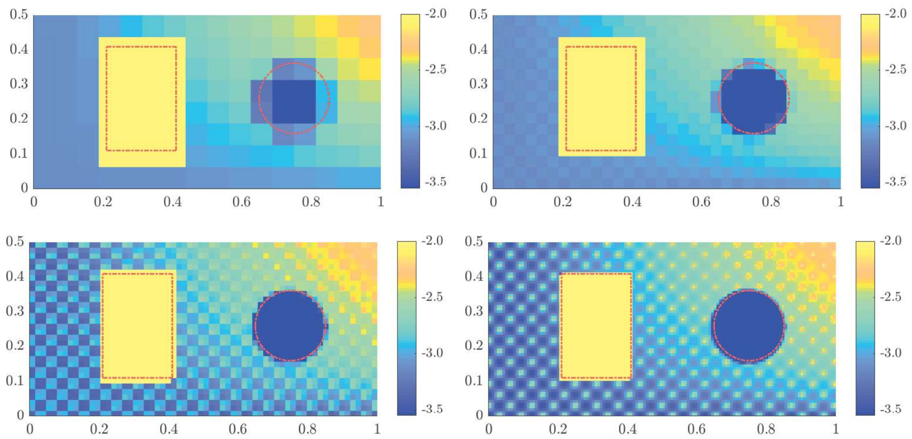

FIG. 5. *Coarse-scale permeability distribution (Log_{10} scale) starting with a coarse grid of 16×8 cells. The red lines indicates the original location of the low permeability zone ($\mathbf{K}^\varepsilon = 10^{-7}$) and high permeability zone ($\mathbf{K}^\varepsilon = 10^{-2}$).*

with a dashed lines the original location of the low and high permeability areas. The numerical solution of the lineal upscaled problem (5.1) is showed in Figure 6. The upscaled solution is computed using the mesh adaptivity described in Section 4 using the threshold for the mesh adaptivity $\Theta = 0.5$. At the end of the adaptive process, the relative L^2-error of the upscaled pressure p_{H_n} is 1.6% using only the 14.7% of the original degrees of freedom.

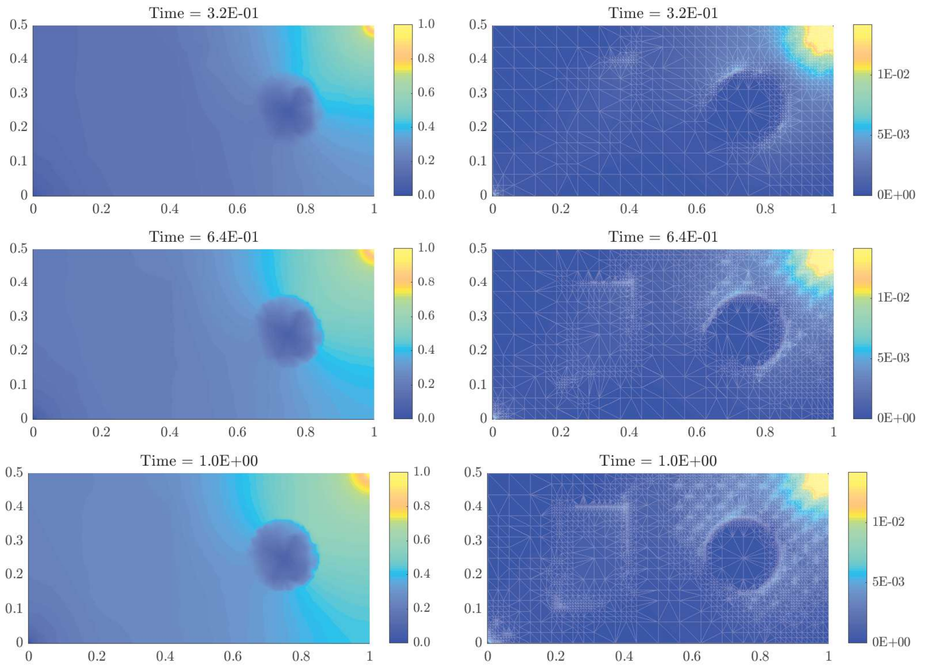

FIG. 6. *Adaptive homogenization at* $t = 16\Delta t$, $32\Delta t$, $50\Delta t$. *Pressure* p_{H_n} *(left) and magnitude of the velocity field* $\|\boldsymbol{u}_{H_n}\|_2$ *(right) over meshes with* 2.367, 5.950 *and* 9.659 *coarse elements.*

Furthermore, after the adaptivity process we obtain a refined version of the permeability field and Figure 7 shows the result of the refined permeability at $t = 1$.

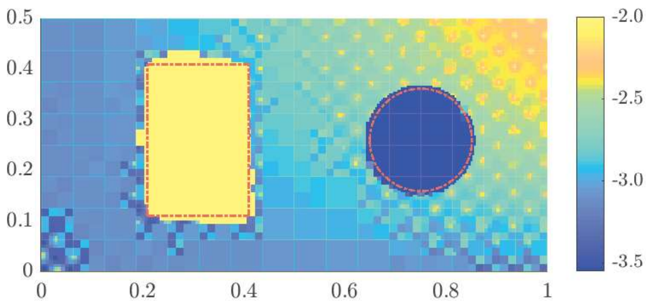

FIG. 7. *Refined permeability field at* $t = 1$ *(*Log_{10} *scale).*

Concerning the behaviour of the non-linear solver, our test case is an example where the convergence of the Newton's method highly depends of the initial guess. However the convergence of the L-scheme is not optimal; i.e., even though the L-scheme converges we do not want to lose the quadratic convergence of the Newton's method. To compute the solution of the Figure 6 the linear solver using only the L-scheme reaches the threshold $\|\delta(p_H)\|_2 < 10^{-10}$ after an average of 70 iterations. In order to improve the linear solver we use a mixed strategy (see [9, 29]). The target is to construct an initial solution that suits a non-problematic starting point for the Newton's method. In this case we used the L-scheme until $\|\delta(p_H)\|_2 < 10^{-2}$ and then the classic Newton's method until one reaches $\|\delta(p_H)\|_2 < 10^{-10}$ (see Figure 8).

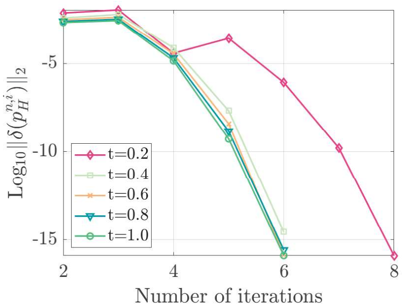

FIG. 8. *Convergence of the residual in the non-linear solver. Results for four different times steps using the L-scheme with $\mathfrak{L} = 1.5\frac{\mathcal{R}}{2}$ and Newton's method afterwards.*

6.2. Non-periodic case. Here we consider a highly heterogeneous and non-periodic medium. We utilize the data of the SPE Comparative Solution Projects [19]. This provides a vehicle for independent comparison of methods and a recognized suite of test datasets for specific problems. Our isotropic permeability field $\mathbf{K}^\varepsilon$ is defined by the top field of SPE10th data set (see Figure 9).

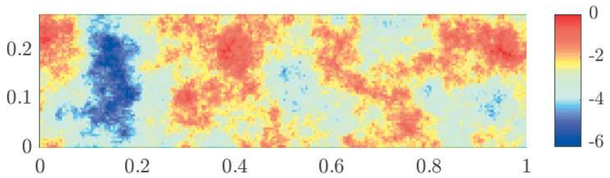

FIG. 9. *Fine scale permeability distribution for SPE10th-TopLayer (Log_{10} scale).*

The macro-scale domain is a two-dimensional rectangle (see Figure 9). External boundaries are impermeable; i.e., we take no-flux boundary conditions. The domain is initialized with pressure $p_0 = 0$. A source and a sink are placed in the lower-left and the upper-right corners, having fixed pressures of 1 and 0, respectively.

Moreover, the volumetric concentration is $b^\varepsilon(\mathbf{x}, (p^\varepsilon)) = \mathcal{R}(p^\varepsilon)^3$. Here $\mathcal{R}$ is defined as in subsection 6.1. For the time discretization we take $T = 1$ with $\Delta t = 0.02$ and the parameter for the non-lineal solver is $\mathfrak{L} = 1.5\frac{\mathcal{R}}{2} \geq \frac{\max\left(3\mathcal{R}(p^\varepsilon)^2\right)}{2}$.

The adaptivity criteria for the dynamic mesh refinement, described in Section 4, is $\Theta = 0.2$. In this case we choose a value of Θ smaller than in subsection 6.1 because we address to capture more changes in the flux and those changes are related with the heterogeneity of the medium. To solve the problem (5.1) with the resolution of Figure 9 we construct a grid with 26.400 elements in a homogeneous triangular mesh $(\mathfrak{T}_{h^\varepsilon})$. In Figure 10 we show the reference solution $(p_{h^\varepsilon}, \mathbf{u}_{h^\varepsilon})$.

Using a coarse grid of 55×15 squares where we compute the first effective permeability field. This coarse grid corresponds to a macro-scale mesh with 1.650 triangular

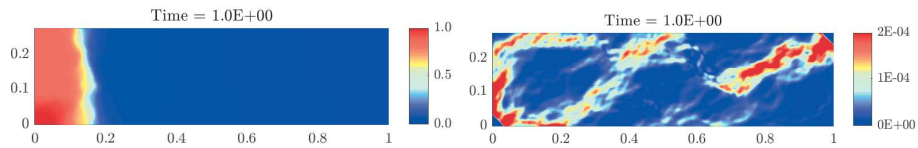

FIG. 10. *Fine scale pressure p_h (left) and (right) magnitude of the velocity field $\|\boldsymbol{u}_h\|_2$.*

elements. In Figure 11 we show the first component ($\mathbf{K}^{\star}_{1,1}$) of the coarse-scale permeability field and this distribution is used afterwards to compute the first step of the adaptivity procedure.

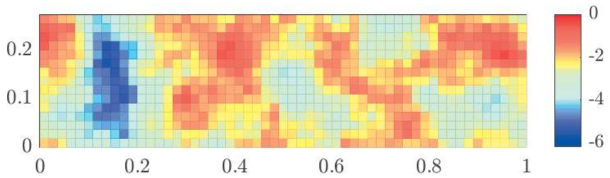

FIG. 11. *Coarse-scale permeability distribution (Log_{10} scale).*

In Figure 12 we show the difference between the effective permeabilities computed with homogenization and using the harmonic average. The difference between these strategies is higher in zones with high permeability and one can point out that the harmonic average always underestimate the permeability. This is problematic because the high permeability regions are regions where one should increase the accuracy of the effective parameter in order to have better numerical solutions. When we compute the numerical solution of (5.1) using the harmonic average of the permeability the relative L^2-error of the pressure is 12.3%.

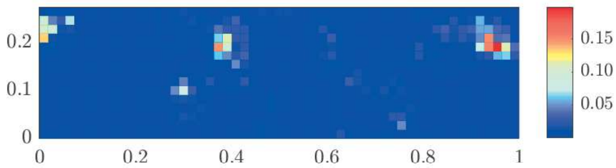

FIG. 12. *Difference between the coarse-scale effective permeabilities using homogenization vs harmonic average.*

Figure 13 shows the numerical solution of the upscaled problem (5.1) using the mesh adaptivity described in section 4. At the end of the adaptive process, the relative L^2-error of the upscaled pressure p_H is 4.72% using only the 16.5% of the original degrees of freedom. Furthermore, using the adaptivity process we obtain a refined version of the permeability field. Figure 14 shows the result of the permeability field after the refinement process.

Finally, in Figure 15 we show the convergence of the norm of the residual $\delta(p_H)$ when one use a combination between the L-scheme and Newton's method. Here we use a mixed strategy (see [29]) to construct an initial solution that suits a non-problematic starting point for the Newton's method. In this case we use the L-scheme until $\|\delta(p_H)\|_2 < 10^{-2}$ and then the classic Newton's method until one reaches $\|\delta(p_H)\|_2 < 10^{-10}$ and as we see in Figure 15 the quadratic convergence of the newton's method is recovered.

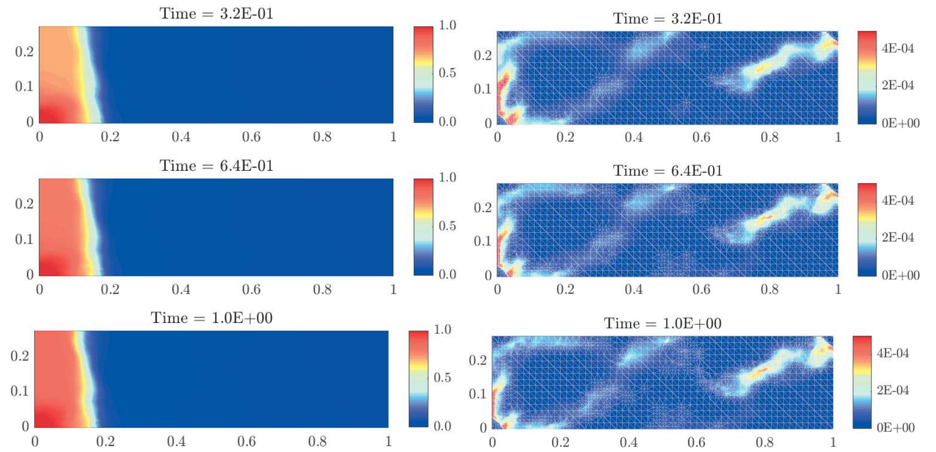

FIG. 13. *Adaptive homogenization at* $t = 16\Delta t$, $32\Delta t$, $50\Delta t$. *Pressure* p_{H_n} *(left) and (right) magnitude of the velocity field* $\|\boldsymbol{u}_{H_n}\|_2$ *over meshes with* 2.701, 3.573 *and* 4.353 *coarse elements.*

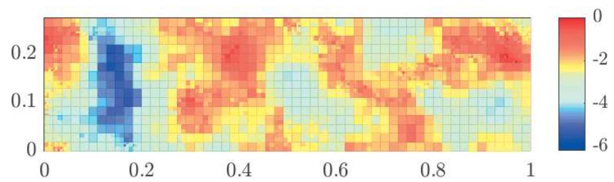

FIG. 14. *Refined permeability field at* $t = 1$ *(*Log_{10} *scale).*

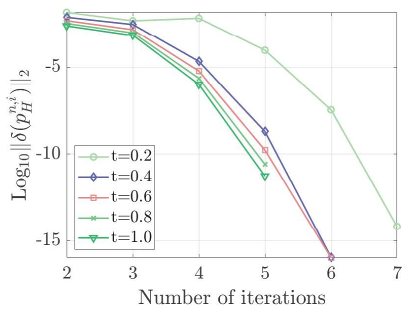

FIG. 15. *Convergence of the residual in the non-linear solver. Results for five different times steps using the L-scheme with* $\mathfrak{L} = 1.5\frac{\mathcal{R}}{2}$ *and Newton's method afterwards.*

7. Conclusions. We have proposed a numerical scheme based on homogenization to solve a non-linear parabolic equation with highly oscillatory characteristics. The discrete non-linear system is obtained by a backward Euler and lowest order Raviart-Thomas mixed finite element discretization. Our approach utilizes a local mesh refinement that leads to the computation of the effective parameters locally through decoupled cell problems. With this we achieved to improve the accuracy of the solution without compromising the efficiency of the method. The adaptivity is based on the idea that the upscaled parameters are updated only when it is necessary. Moreover, to illustrate the performance we have presented two general examples. We construct a periodic case to show the history of convergence of the error when the scale separation tends to zero. In the non-periodic case we used a benchmark from the SPE10th project and we showed that the homogenization can be used in general cases.

In addition to the aforementioned, we combined the standard Newton's method and the L-scheme to improve the behaviour of the non-linear solvers. We presented a combination of techniques that lead to a very efficient numerical scheme. It is relevant to mention that besides the theory mentioned in this paper the applicability of this strategy is vast. Extensions of our adaptive algorithm including more complex micro-scale models are applicable. Those include from reactive transport up to moving interfaces affecting the structure of the micro-scale.

Acknowledgements. The authors gratefully acknowledge financial support from the Research Foundation - Flanders (FWO) through the Odysseus programme (Project G0G1316N). In addition, we wish to thank Professor Mary F. Wheeler, Professor Ivan Yotov and Professor Hadi Hajibeygi who made valuable suggestions or who have otherwise contributed to the ideas behind this manuscript. Part of this work was elaborated during the stay of the first author in the University of Bergen supported by the Research Foundation - Flanders (FWO) through a travel grant for a short stay abroad.

REFERENCES

[1] A. Abdulle and A. Nonnenmacher, *A short and versatile finite element multiscale code for homogenization problems*, Computer Methods in Applied Mechanics and Engineering, 198 (2009), pp. 2839–2859.

[2] A. Abdulle and A. Nonnenmacher, *Adaptive finite element heterogeneous multiscale method for homogenization problems*, Computer Methods in Applied Mechanics and Engineering, 200 (2011), pp. 2710–2726.

[3] A. Abdulle, E. Weinan, B. Engquist, and E. Vanden-Eijnden, *The heterogeneous multiscale method*, Acta Numerica, 21 (2012), pp. 1–87.

[4] H. W. Alt and S. Luckhaus, *Quasilinear elliptic-parabolic differential equations*, Mathematische Zeitschrift, 183 (1983), pp. 311–341.

[5] Y. Amanbek, G. Singh, M. F. Wheeler, and H. van Duijn, *Adaptive numerical homogenization for upscaling single phase flow and transport*, ICES Report, 12 (2017), p. 17.

[6] T. Arbogast, G. Pencheva, M. F. Wheeler, and I. Yotov, *A multiscale mortar mixed finite element method*, Multiscale Modeling & Simulation, 6 (2007), pp. 319–346.

[7] J. Bear and Y. Bachmat, *Introduction to modeling of transport phenomena in porous media*, vol. 4, Springer Science & Business Media, 2012.

[8] L. Bergamaschi and M. Putti, *Mixed finite elements and Newton-type linearizations for the solution of Richards' equation*, International journal for numerical methods in engineering, 45 (1999), pp. 1025–1046.

[9] J. W. Both, K. Kumar, J. M. Nordbotten, I. S. Pop, and F. A. Radu, *Iterative linearisation schemes for doubly degenerate parabolic equations*, in Numerical Mathematics and Advanced Applications ENUMATH 2017, F. A. Radu, K. Kumar, I. Berre, J. M. Nordbotten, and I. S. Pop, eds., Springer International Publishing, pp. 49–63.

[10] F. Brezzi and M. Fortin, *Mixed and hybrid finite element methods*, vol. 15, Springer Science & Business Media, 2012.

[11] C. Bringedal, I. Berre, I. S. Pop, and F. A. Radu, *Upscaling of non-isothermal reactive porous media flow with changing porosity*, Transport in Porous Media, 114 (2016), pp. 371–393.

[12] H. T. Cao and X. Y. Yue, *Homogenization of a nonlinear degenerate parabolic differential equation*, Acta Mathematica Sinica. English Series, 29 (2013), p. 1429.

[13] C. Carstensen, *All first-order averaging techniques for a posteriori finite element error control on unstructured grids are efficient and reliable*, Mathematics of Computation, 73 (2004), pp. 1153–1165.

[14] C. Carstensen, *A unifying theory of a posteriori finite element error control*, Numerische Mathematik, 100 (2005), pp. 617–637.

[15] C. Carstensen and S. A. Funken, *A posteriori error control in low-order finite element discretisations of incompressible stationary flow problems*, Math. Comput, 70 (1999), pp. 1353–1381.
[16] C. Carstensen and R. Hoppe, *Error reduction and convergence for an adaptive mixed finite element method*, Mathematics of Computation, 75 (2006), pp. 1033–1042.
[17] M. A. Celia, E. T. Bouloutas, and R. L. Zarba, *A general mass-conservative numerical solution for the unsaturated flow equation*, Water resources research, 26 (1990), pp. 1483–1496.
[18] S. Chen, W. E, and C.-W. Shu, *The heterogeneous multiscale method based on the discontinuous Galerkin method for hyperbolic and parabolic problems*, Multiscale Modeling & Simulation, 3 (2005), pp. 871–894.
[19] M. A. Christie and M. J. Blunt, *Tenth SPE comparative solution project: A comparison of upscaling techniques*, Society of Petroleum Engineers, 2001.
[20] D. Cioranescu and P. Donato, *An Introduction to Homogenization*, Oxford lecture series in mathematics and its applications, Oxford University Press.
[21] M. Cusini, C. van Kruijsdijk, and H. Hajibeygi, *Algebraic dynamic multilevel (ADM) method for fully implicit simulations of multiphase flow in porous media*, Journal of Computational Physics, 314 (2016), pp. 60–79.
[22] R. J. de Moraes, J. R. Rodrigues, H. Hajibeygi, and J. D. Jansen, *Multiscale gradient computation for flow in heterogeneous porous media*, Journal of Computational Physics, 336 (2017), pp. 644–663.
[23] B. Ganis, G. Pencheva, and M. F. Wheeler, *Adaptive mesh refinement with an enhanced velocity mixed finite element method on semi-structured grids using a fully coupled solver*, Computational Geosciences, (2018).
[24] N. Golias and R. Dutton, *Delaunay triangulation and 3D adaptive mesh generation*, Finite Elements in Analysis and Design, 25 (1997), pp. 331– 341. Adaptive Meshing, Part 2.
[25] H. Hajibeygi, G. Bonfigli, M. A. Hesse, and P. Jenny, *Iterative multiscale finite-volume method*, Journal of Computational Physics, 227 (2008), pp. 8604–8621.
[26] U. Hornung, *Homogenization and Porous Media*, vol. 6, Springer Science & Business Media, 1997.
[27] J. Huaiyu, *On the homogenization of degenerate parabolic equations*, Acta Mathematicae Applicatae Sinica, 16 (2000), pp. 100–110.
[28] F. List and F. A. Radu, *A study on iterative methods for solving Richards' equation*, Computational Geosciences, 20 (2016), pp. 341–353.
[29] K. Mitra and I. S. Pop, *A modified l-scheme to solve nonlinear diffusion problems*, Computers & Mathematics with Applications, 77 (2019), pp. 1722–1738.
[30] A. Nandakumaran and M. Rajesh, *Homogenization of a parabolic equation in perforated domain with dirichlet boundary condition*, in Proceedings of the Indian Academy of Sciences-Mathematical Sciences, vol. 112, Springer, 2002, pp. 425–439.
[31] I. S. Pop, F. Radu, and P. Knabner, *Mixed finite elements for the Richards' equation: Linearization procedure*, Journal of computational and applied mathematics, 168 (2004), pp. 365–373.
[32] F. Radu, I. S. Pop, and P. Knabner, *Order of convergence estimates for an Euler implicit, mixed finite element discretization of Richards' equation*, SIAM Journal on Numerical Analysis, 42 (2004), pp. 1452–1478.
[33] F. A. Radu, K. Kumar, J. M. Nordbotten, and I. S. Pop, *A robust, mass conservative scheme for two-phase flow in porous media including hölder continuous nonlinearities*, IMA Journal of Numerical Analysis, 38 (2017), pp. 884–920.
[34] F. A. Radu, J. M. Nordbotten, I. S. Pop, and K. Kumar, *A robust linearization scheme for finite volume based discretizations for simulation of two-phase flow in porous media*, Journal of Computational and Applied Mathematics, 289 (2015), pp. 134–141.
[35] F. A. Radu, I. S. Pop, and P. Knabner, *Error estimates for a mixed finite element discretization of some degenerate parabolic equations*, Numerische Mathematik, 109 (2008), pp. 285–311.
[36] P. Renard and G. De Marsily, *Calculating equivalent permeability: a review*, Advances in water resources, 20 (1997), pp. 253–278.
[37] G. Singh, W. Leung, and M. F. Wheeler, *Multiscale methods for model order reduction of non-linear multiphase flow problems*, Computational Geosciences, (2018), pp. 1–19.
[38] M. Slodicka, *A robust and efficient linearization scheme for doubly nonlinear and degenerate parabolic problems arising in flow in porous media*, SIAM Journal on Scientific Computing, 23 (2002), pp. 1593–1614.
[39] L. Tartar, *The General Theory of Homogenization: A Personalized Introduction*, Springer

Science & Business Media, 2009.
[40] E. Weinan, B. Engquist, and Z. Huang, *Heterogeneous multiscale method: A general methodology for multiscale modeling*, Physical Review B, 67 (2003), p. 092101.
[41] J. A. Wheeler, M. F. Wheeler, and I. Yotov, *Enhanced velocity mixed finite element methods for flow in multiblock domains*, Computational Geosciences, 6 (2002), pp. 315–332.

UHasselt Computational Mathematics Preprint Series

2019

UP-19-04 *M. Bastidas, C. Bringedal, I.S. Pop, F.A. Radu*, **Adaptive numerical homogenization of nonlinear diffusion problems**, 2019

UP-19-03 *K. Kumar, F. List, I.S. Pop, F.A. Radu*, **Formal upscaling and numerical validation of fractured flow models for Richards′ equation**, 2019

UP-19-02 *M.A. Endo Kokubun, A. Muntean, F.A. Radu, K. Kumar, I.S. Pop, E. Keilegavlen, K. Spildo*, **A pore-scale study of transport of inertial particles by water in porous media**, 2019

UP-19-01 *Carina Bringedal, Lars von Wolff, and Iuliu Sorin Pop*, **Phase field modeling of precipitation and dissolution processes in porous media: Upscaling and numerical experiments**, 2019

2018

UP-18-09 *David Landa-Marbán, Gunhild Bodtker, Kundan Kumar, Iuliu Sorin Pop, Florin Adrian Radu*, **An upscaled model for permeable biofilm in a thin channel and tube**, 2018

UP-18-08 *Vo Anh Khoa, Le Thi Phuong Ngoc, Nguyen Thanh Long*, **Existence, blow-up and exponential decay of solutions for a porous-elastic system with damping and source terms**, 2018

UP-18-07 *Vo Anh Khoa, Tran The Hung, Daniel Lesnic*, **Uniqueness result for an age-dependent reaction-diffusion problem**, 2018

UP-18-06 *Koondanibha Mitra, Iuliu Sorin Pop*, **A modified L-Scheme to solve nonlinear diffusion problems**, 2018

UP-18-05 *David Landa-Marban, Na Liu, Iuliu Sorin Pop, Kundan Kumar, Per Pettersson, Gunhild Bodtker, Tormod Skauge, Florin A. Radu*, **A pore-scale model for permeable biofilm: numerical simulations and laboratory experiments**, 2018

UP-18-04 *Florian List, Kundan Kumar, Iuliu Sorin Pop and Florin A. Radu*, **Rigorous upscaling of unsaturated flow in fractured porous media**, 2018

UP-18-03 *Koondanibha Mitra, Hans van Duijn*, **Wetting fronts in unsaturated porous media: the combined case of hysteresis and dynamic capillary**, 2018

UP-18-02 *Xiulei Cao, Koondanibha Mitra*, **Error estimates for a mixed finite element discretization of a two-phase porous media flow model with dynamic capillarity**, 2018

UP-18-01 *Klaus Kaiser, Jonas Zeifang, Jochen Schütz, Andrea Beck and Claus-Dieter Munz*, **Comparison of different splitting techniques for the isentropic Euler equations**, 2018

2017

UP-17-12 *Carina Bringedal, Tor Eldevik, Øystein Skagseth and Michael A. Spall*, **Structure and forcing of observed exchanges across the Greenland-Scotland Ridge**, 2017

UP-17-11 *Jakub Wiktor Both, Kundan Kumar, Jan Martin Nordbotten, Iuliu Sorin Pop and Florin Adrian Radu*, **Linear iterative schemes for doubly degenerate parabolic equations**, 2017

UP-17-10 *Carina Bringedal and Kundan Kumar*, **Effective behavior near clogging in upscaled equations for non-isothermal reactive porous media flow**, 2017

UP-17-09 *Alexander Jaust, Balthasar Reuter, Vadym Aizinger, Jochen Schütz and Peter Knabner*, **FESTUNG: A MATLAB / GNU Octave toolbox for the discontinuous Galerkin method. Part III: Hybridized discontinuous Galerkin (HDG) formulation**, 2017

UP-17-08 *David Seus, Koondanibha Mitra, Iuliu Sorin Pop, Florin Adrian Radu and Christian Rohde*, **A linear domain decomposition method for partially saturated flow in porous media**, 2017

UP-17-07 *Klaus Kaiser and Jochen Schütz*, **Asymptotic Error Analysis of an IMEX Runge-Kutta method**, 2017

UP-17-06 *Hans van Duijn, Koondanibha Mitra and Iuliu Sorin Pop*, **Travelling wave solutions for the Richards equation incorporating non-equilibrium effects in the capillarity pressure**, 2017

UP-17-05 *Hans van Duijn and Koondanibha Mitra*, **Hysteresis and Horizontal Redistribution in Porous Media**, 2017

UP-17-04 *Jonas Zeifang, Klaus Kaiser, Andrea Beck, Jochen Schütz and Claus-Dieter Munz*, **Efficient high-order discontinuous Galerkin computations of low Mach number flows**, 2017

UP-17-03 *Maikel Bosschaert, Sebastiaan Janssens and Yuri Kuznetsov*, **Switching to nonhyperbolic cycles from codim-2 bifurcations of equilibria in DDEs**, 2017

UP-17-02 *Jochen Schütz, David C. Seal and Alexander Jaust*, **Implicit multiderivative collocation solvers for linear partial differential equations with discontinuous Galerkin spatial discretizations**, 2017

UP-17-01 *Alexander Jaust and Jochen Schütz*, **General linear methods for time-dependent PDEs**, 2017

2016

UP-16-06 *Klaus Kaiser and Jochen Schütz*, **A high-order method for weakly compressible flows**, 2016

UP-16-05 *Stefan Karpinski, Iuliu Sorin Pop, Florin A. Radu*, **A hierarchical scale separation approach for the hybridized discontinuous Galerkin method**, 2016

UP-16-04 *Florin A. Radu, Kundan Kumar, Jan Martin Nordbotten, Iuliu Sorin Pop*, **Analysis of a linearization scheme for an interior penalty discontinuous Galerkin method for two phase flow in porous media with dynamic capillarity effects** , 2016

UP-16-03 *Sergey Alyaev, Eirik Keilegavlen, Jan Martin Nordbotten, Iuliu Sorin Pop*, **Fractal structures in freezing brine**, 2016

UP-16-02 *Klaus Kaiser, Jochen Schütz, Ruth Schöbel and Sebastian Noelle*, **A new stable splitting for the isentropic Euler equations**, 2016

UP-16-01 *Jochen Schütz and Vadym Aizinger*, **A hierarchical scale separation approach for the hybridized discontinuous Galerkin method**, 2016